Supporting Information for

Enhanced Tetrabromobisphenol A Debromination by Nanoscale Zero Valent Iron Particles Sulfidated with S^0 Dissolved in Ethanol

Heli Wang[a,b], Yin Zhong[a,*], Xifen Zhu[a,b], Dan Li[a,b,d], Yirong Deng[a,b,e], Weilin Huang[c], Ping'an Peng[a]

[a] State Key Laboratory of Organic Geochemistry, Guangdong Provincial Key Laboratory of Environmental Protection and Resources and Utilization, Guangdong-Hong Kong-Maco Joint Laboratory for Environmental Pollution and Control, Guangzhou Institute of Geochemistry, Chinese Academy of Sciences, Guangzhou 510640, China

[b]University of Chinese Academy of Sciences, Beijing 100049, China

[c]Department of Environmental Sciences, Rutgers, The State University of New Jersey, 14 College Farm Road, New Brunswick, NJ 08901 USA

[d]School of Environment and Civil Engineering, Dongguan University of Technology, Dongguan 523808, China

[e]Guangdong Key Laboratory of Contaminated Sites Environmental Management and Remediation, Guangdong Provincial Academy of Environmental Science, Guangzhou 510045, China

*Corresponding author
State Key Laboratory of Organic Geochemistry
Guangzhou Institute of Geochemistry
Chinese Academy of Sciences
Wushan, Guangzhou 510640, China
Tel.: +86-20-85290142
Fax: +86-20-85290117
E-mail: zhongyin@gig.ac.cn

Summary

Fig. S9. Effect of S/Fe molar ratio on the transformation of TBBPA by S-nZVI^{S}. Lines are pseudo-first order fittings of data points.The initial concentration of S-nZVI^{S} and TBBPA were 2.3 g L^{-1} and 20 mg L^{-1}, respectively.

Fig. S10. Proposed debromination pathways of TBBPA by nZVI and S-nZVI^{S} with different S/Fe molar ratios.

Fig. S11. Transformation kinetics of TBBPA by S-nZVI^{Na_2S} and S-nZVI^{Na_2S_2O_4}. The solid lines represent the simulated curves based on the pseudo-first-order reaction kinetic model. The initial concentration of S-nZVI particles and TBBPA are 2.3 g L^{-1} and 20 mg L^{-1}, respectively.

Fig. S12. Detailed XPS survey of the region for Fe 2p3/2 (A, B) and S 2p (C, D) from S-nZVI$^{Na_2S_2O_4\text{-}0.5}$ (A, C) and S-nZVI$^{Na_2S\text{-}0.025}$ (B, D).

Fig. S13. Transformation kinetics of TBBPA by S-nZVI$^{S\text{-}0.025}$(S-) under different real waters. The solid lines represent the simulated curves based on the pseudo-first-order reaction kinetic model. The initial concentration of S-nZVI$^{S\text{-}0.025}$ particles and TBBPA are 2.3 g L^{-1} and 5 mg L^{-1}, respectively.

Table S1. Binding energy and relative peak area of XPS peaks of Fe($2p_{3/2}$) and S($2p_{3/2}$) elements on the surface of nZVI and S-nZVI^{S} samples

Table S2. Theoretical and actual S/Fe and relative atomic percentage of Fe, S, O, and C of S-nZVI^{S} at different S/Fe molar ratios.

Table S3. Summary of parameters obtained from fitting HER data with the First-order passivation of Fe^0 model with k as global.

Table S4. Summary of parameters obtained from fitting HER data to the Replacement of reactive phases model.

Text S1. List of chemicals and reagents.

TBBPA standard (97%), bisphenol A (BPA) standard (99%) were purchased from Alfa Aesar (Ward Hill, USA). The standards of debromination products (i.e., tri-BBPA, di-BBPA, mono-BBPA) are synthesized in Dr. Zhiqiang Yu's of Guangzhou Institute of Geochemistry, Chinese Academy of Sciences. Ferrous chloride tetrahydrate ($FeCl_2 \cdot 4H_2O$, 99.5%-101.0%), sublimed sulfur (S, 99.5%) and concentrated HCl (guaranteed reagent, 37%, w/w) were obtained from Guangzhou Chemical Reagents Factory (Guangzhou, China). Sodium borohydride ($NaBH_4$, 98%) were purchased from Sinopharm Chemical Reagent Co., Ltd (Shanghai, China). Ethanol (AR, 99.7%) was supplied by Shanghai Titan Scientific Co.,Ltd. HPLC-grade methanol was obtained from Merck (Darmstadt, Germany). Ultra high purity compressed nitrogen gas was purchased from Foshan MS Messer Gas Co.,Ltd (Guangzhou, China). The ultrapure water (resistivity: 18.2 MΩ cm) was deoxygenated with high purity nitrogen (99.999%) for 40 min and was then taken into anaerobic chamber to prepare aqueous solutions.

Fig. S1. SEM micrographs and for S-nZVI^{s} at different S/Fe molar ratios. (A) nZVI, (B) S/Fe = 0.025, (C) S/Fe = 0.25.

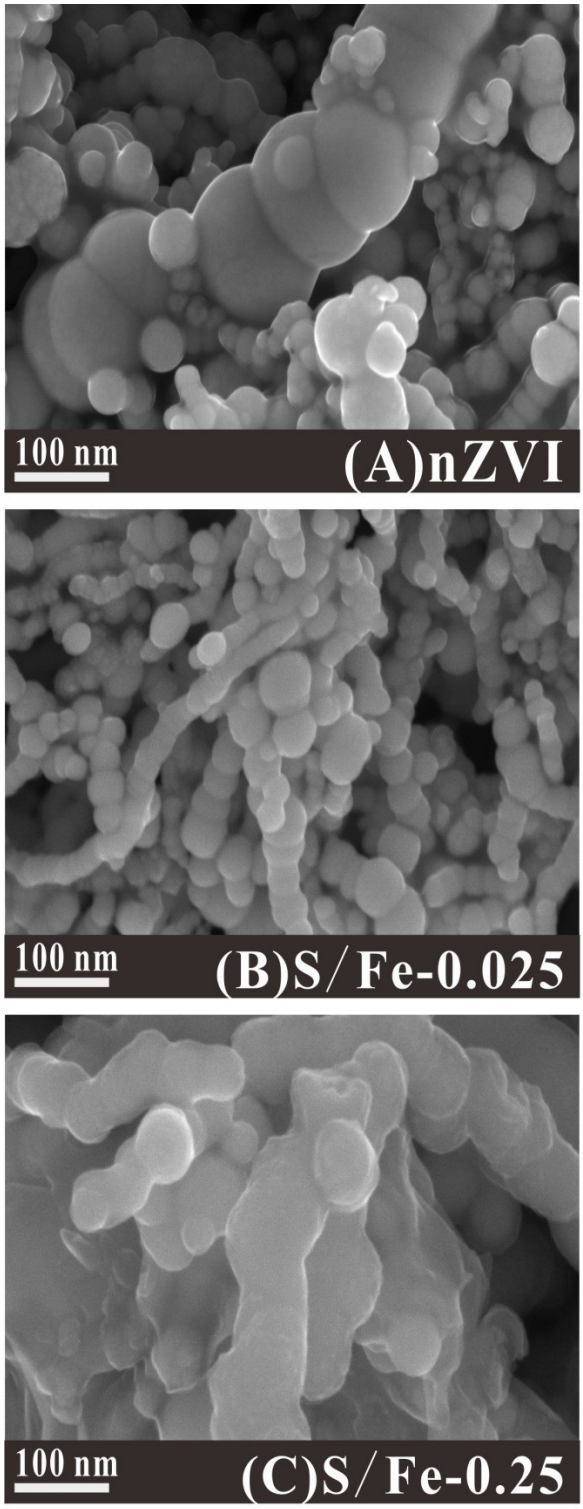

Fig. S2. The EDS spectra of nZVI and S-nZVI^{S} at different S/Fe molar ratios. (A) nZVI, (B) S/Fe = 0.015; (C) S/Fe = 0.025; (D) S/Fe = 0.05; (E) S/Fe = 0.1; (F) S/Fe = 0.25.

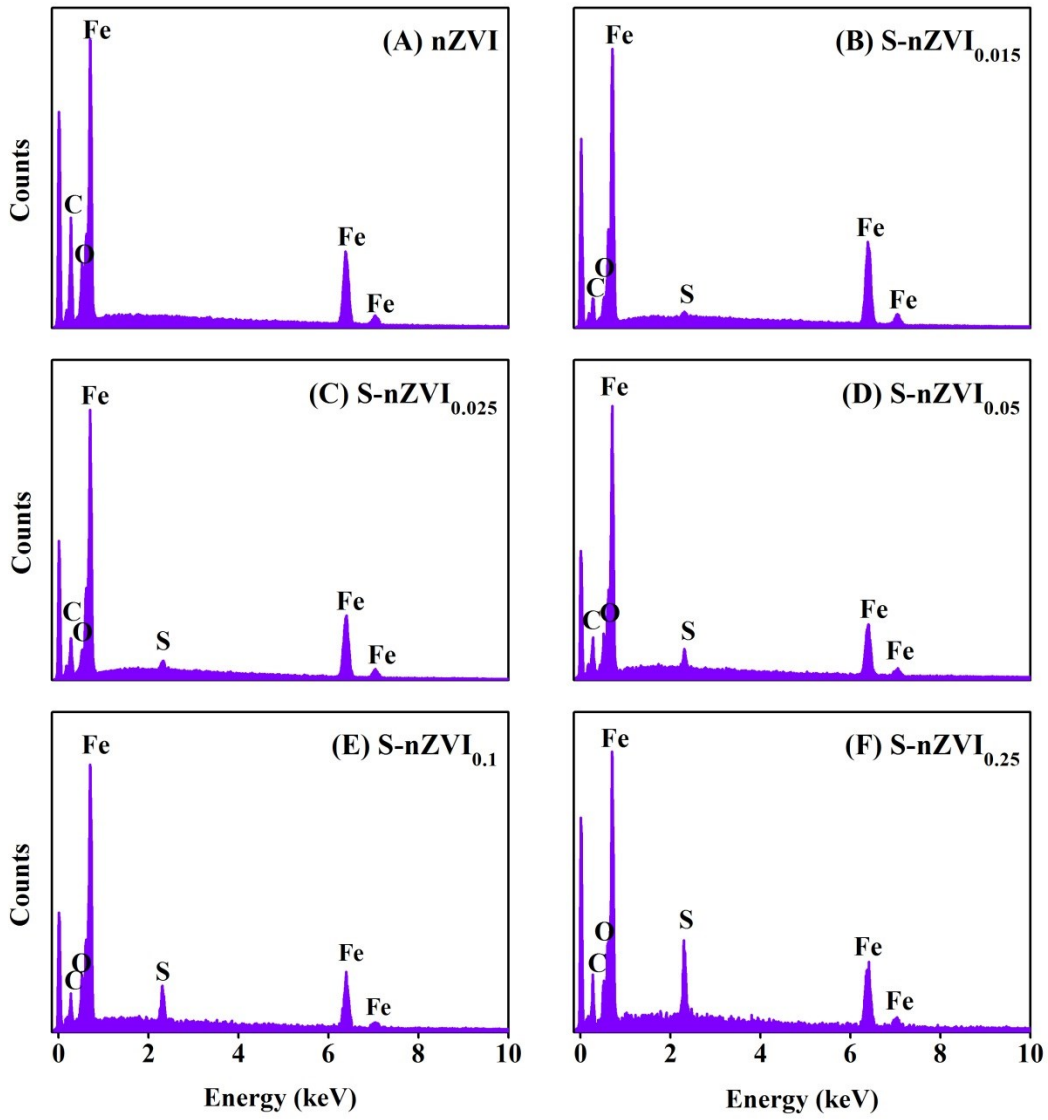

Fig. S3.TEM images of freshly prepared nZVI (A) and S-nZVI^{S} at S/Fe of 0.25 (B).

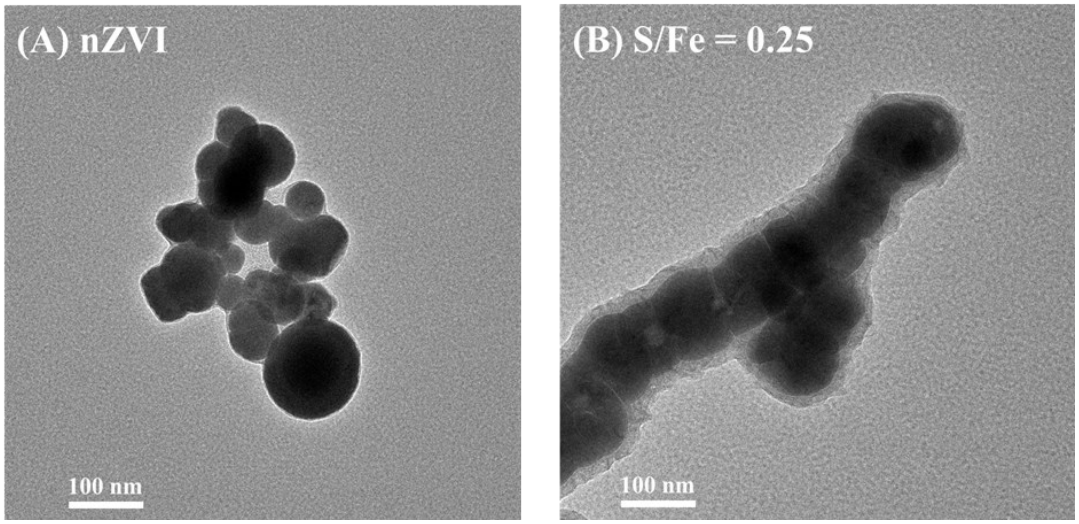

Fig. S4. Detailed XPS survey of the region for S 2p for S-nZVI^{S} at different S/Fe molar ratios. (A) nZVI; (B) S/Fe = 0.015; (C) S/Fe = 0.025; (D) S/Fe = 0.05; (E) S/Fe = 0.1; (F) S/Fe = 0.25.

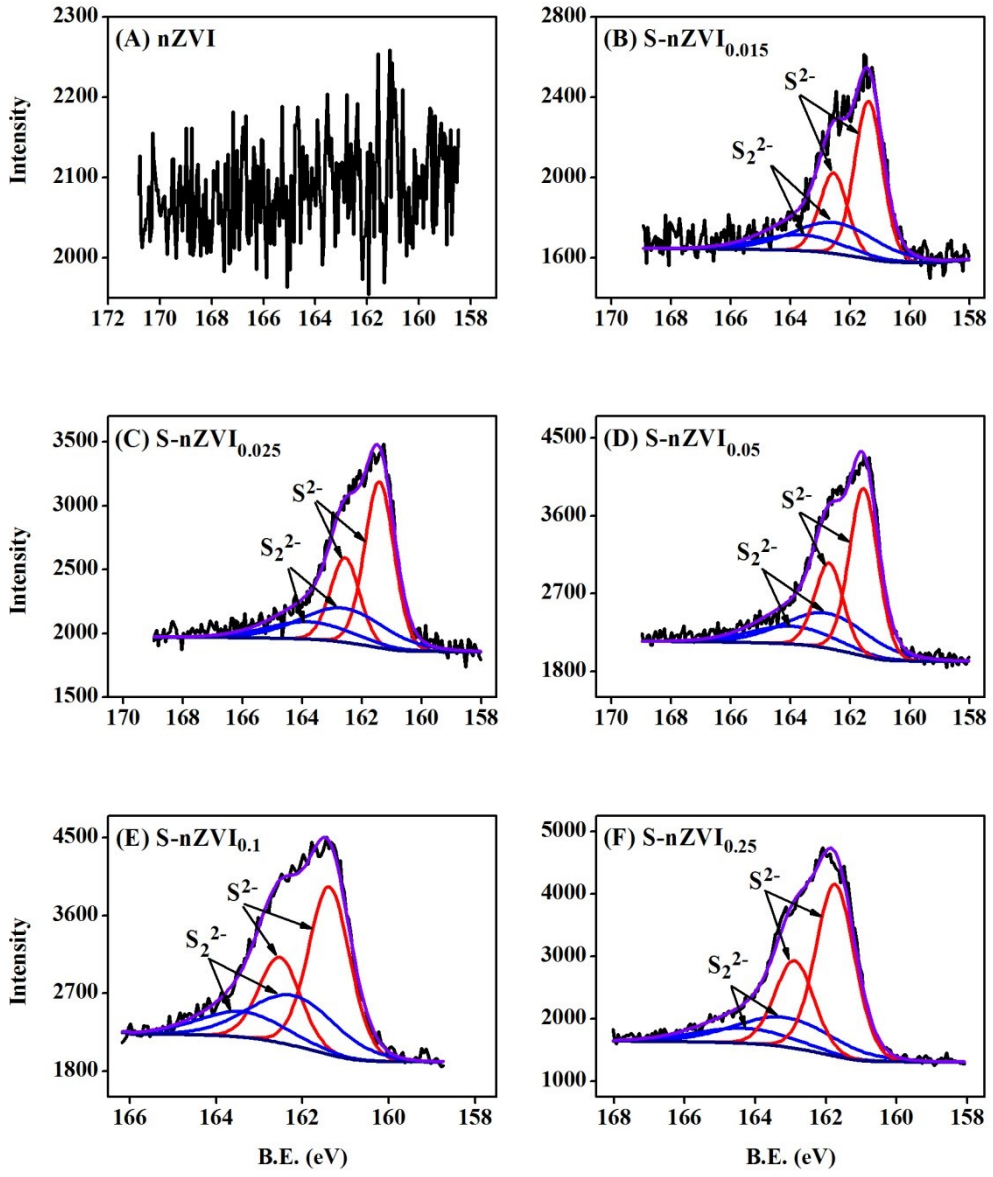

Fig. S5. Detailed XPS survey of the region for Fe $2p_{3/2}$ for S-nZVI^S at different S/Fe molar ratios. (A) nZVI; (B) S/Fe = 0.015; (C) S/Fe = 0.025; (D) S/Fe = 0.05; (E) S/Fe = 0.1; (F) S/Fe = 0.25.

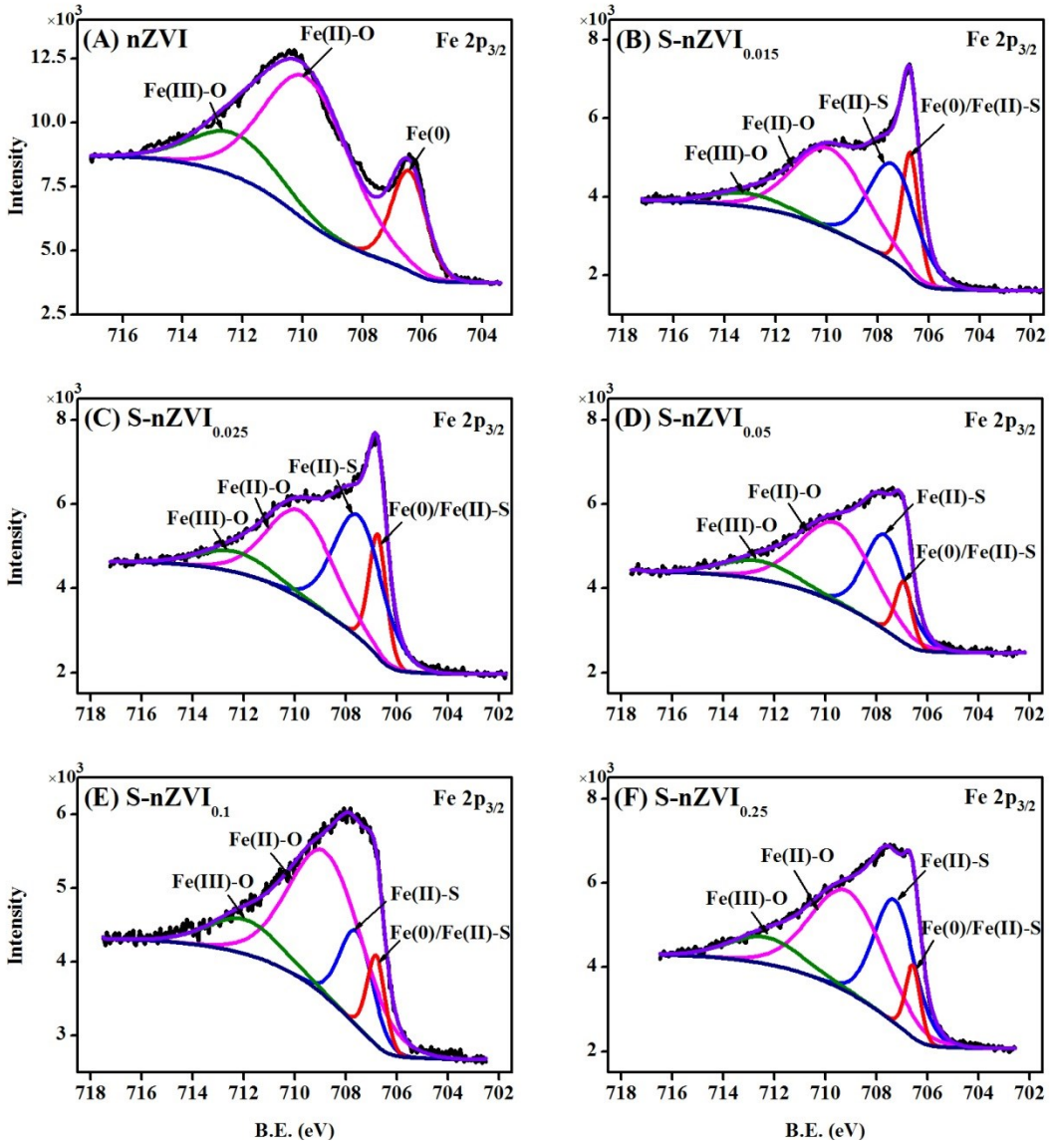

Fig. S6. Hydrodynamic diameter (A), zeta potential (B) and N_2-BET specific surface area (C) of the S-nZVI^S with different extents of sulfidation.

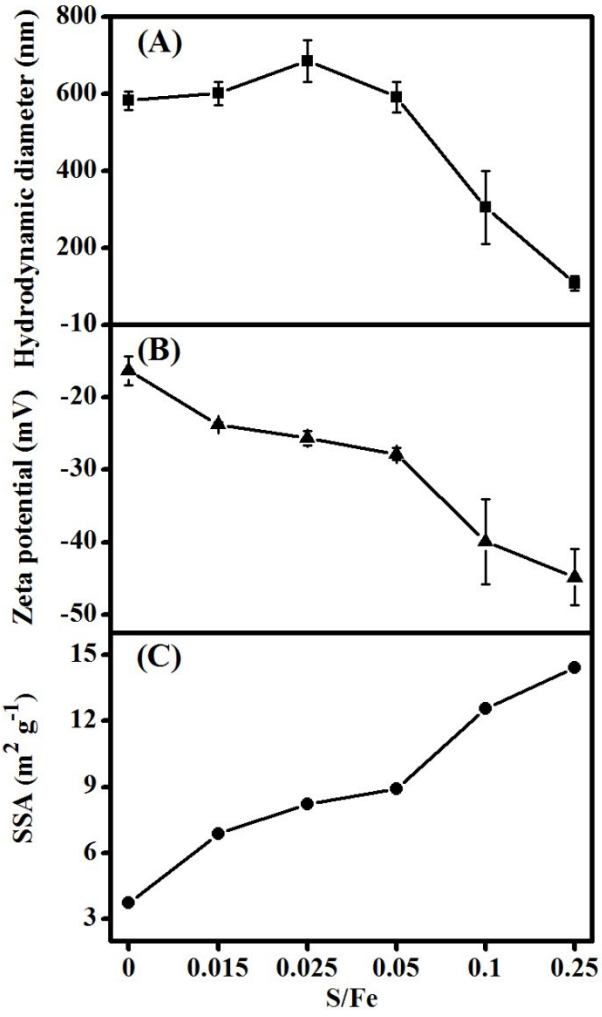

Fig S7. H_2 evolution for S-nZVIS with different S/Fe molar ratios and fit to different models. The initial concentration of S-nZVIS was 2.3 g L^{-1}. (A) First-order passivation of Fe(0) model; (B) Replacement of reactive phases model; (C) Advanced phase replacement model; (D) Independent changes in two reactive phases model.

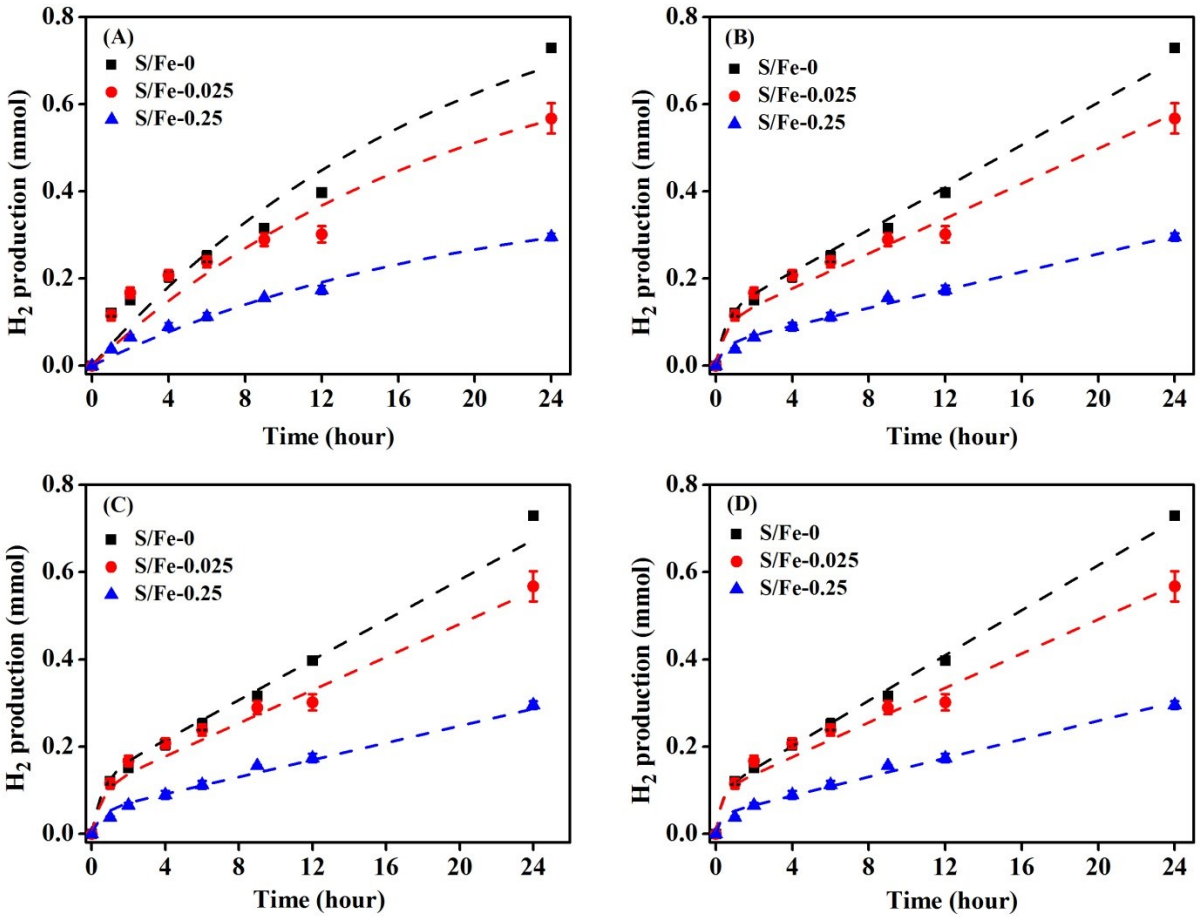

Fig. S8. Change in the pH value of reaction solution during the reaction of S-nZVI$^{S\text{-}0.025}$ with TBBPA. The initial concentration of S-nZVI^{S} and TBBPA are 2.3 g L^{-1} and 20 mg L^{-1}, respectively.

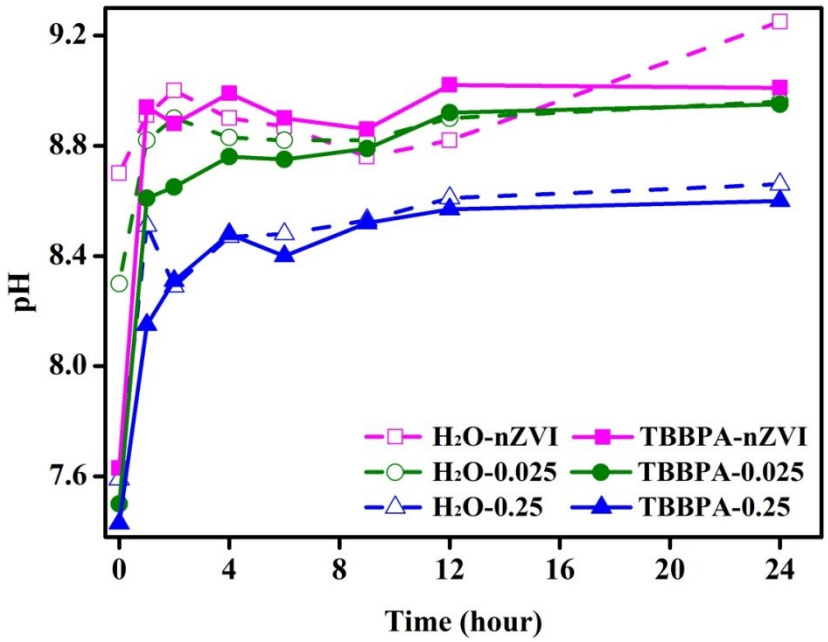

Fig S9. Effect of S/Fe molar ratio on the transformation of TBBPA by S-nZVI^{S}. Lines are pseudo-first order fittings of data points.The initial concentration of S-nZVI^{S} and TBBPA were 2.3 g L^{-1} and 20 mg L^{-1}, respectively.

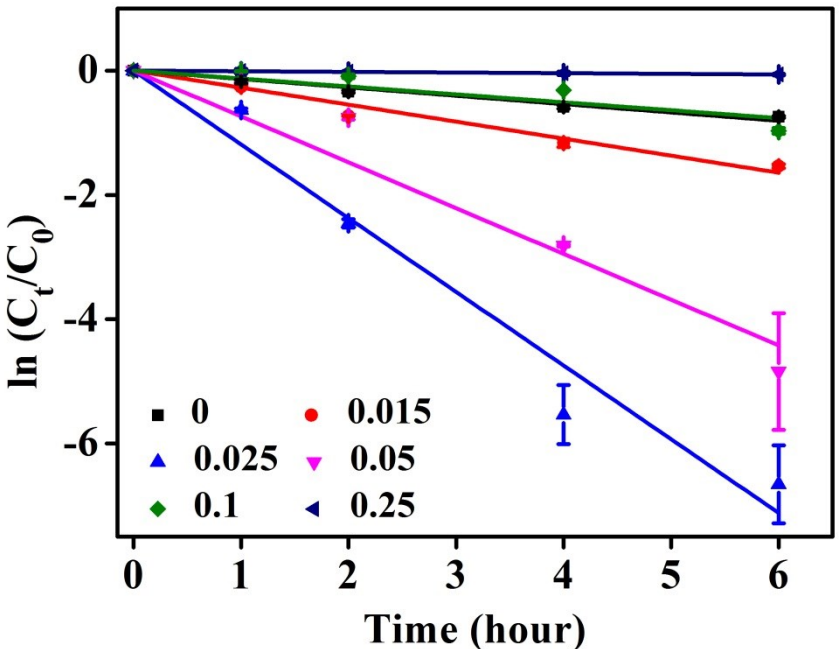

Fig. S10. Proposed debromination pathways of TBBPA by nZVI and S-nZVI^{S} with different S/Fe molar ratios.

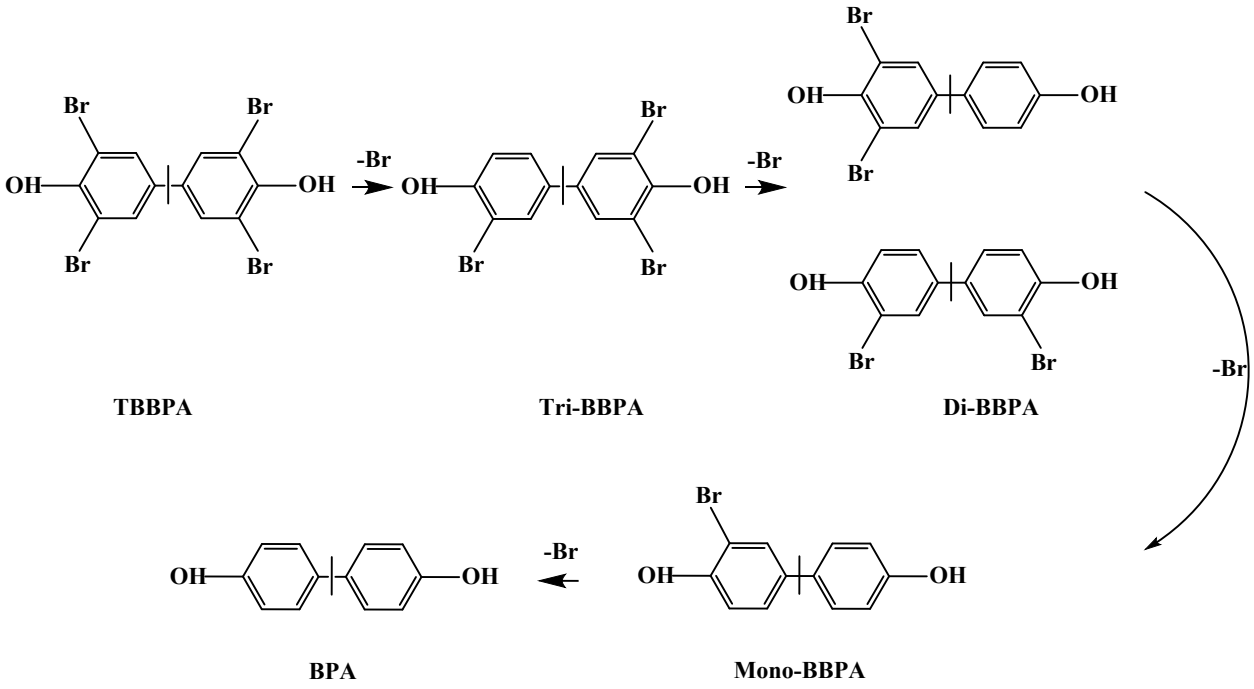

Fig. S11. Transformation kinetics of TBBPA by S-nZVI^{Na_2S} and S-nZVI^{Na_2S_2O_4}. The solid lines represent the simulated curves based on the pseudo-first-order reaction kinetic model. The initial concentration of S-nZVI particles and TBBPA are 2.3 g L^{-1} and 20 mg L^{-1}, respectively.

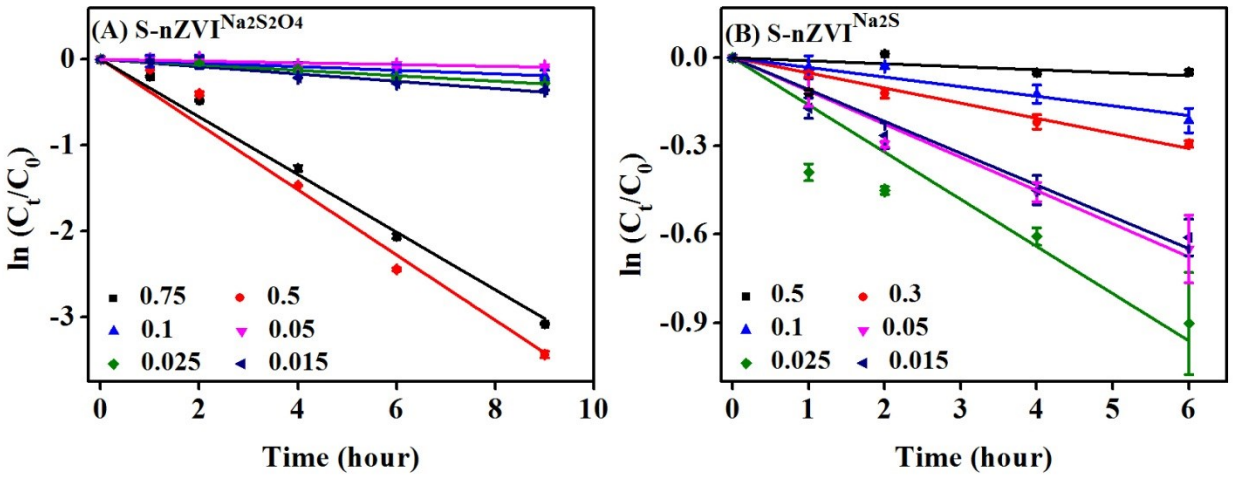

Fig. S12. Detailed XPS survey of the region for Fe 2p3/2 (A, B) and S 2p (C, D) from S-nZVI$^{Na_2S_2O_4\text{-}0.5}$ (A, C) and S-nZVI$^{Na_2S\text{-}0.025}$ (B, D).

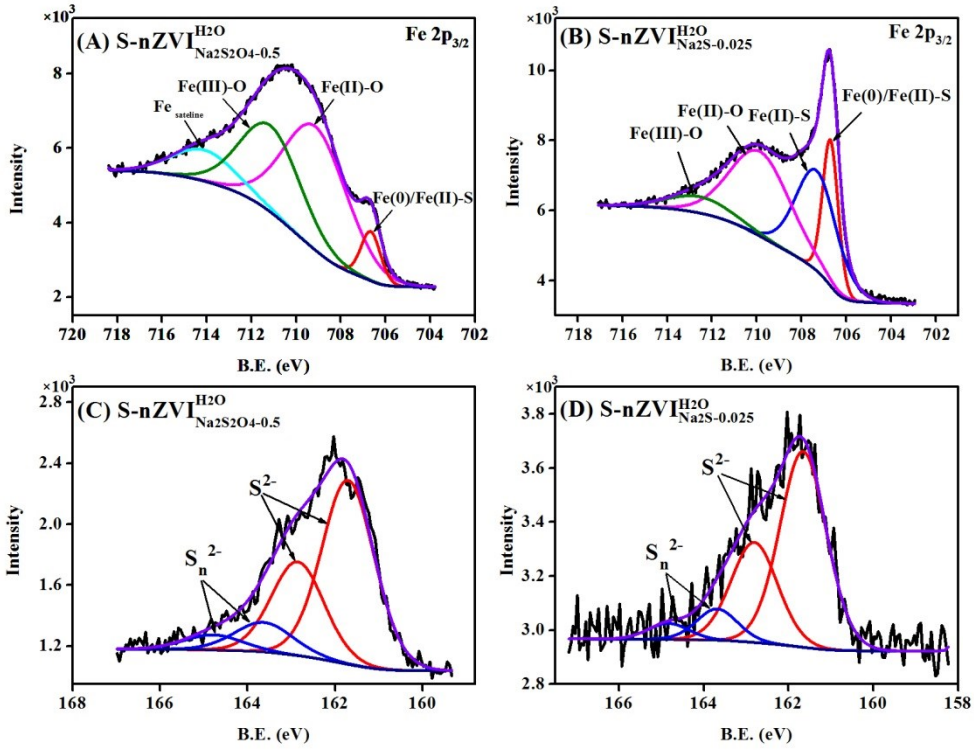

Fig. S13. Transformation kinetics of TBBPA by S-nZVI$^{S\text{-}0.025}$(S-) under different real waters . The solid lines represent the simulated curves based on the pseudo-first-order reaction kinetic model. The initial concentration of S-nZVI$^{S\text{-}0.025}$ particles and TBBPA are 2.3 g L^{-1} and 5 mg L^{-1}, respectively.

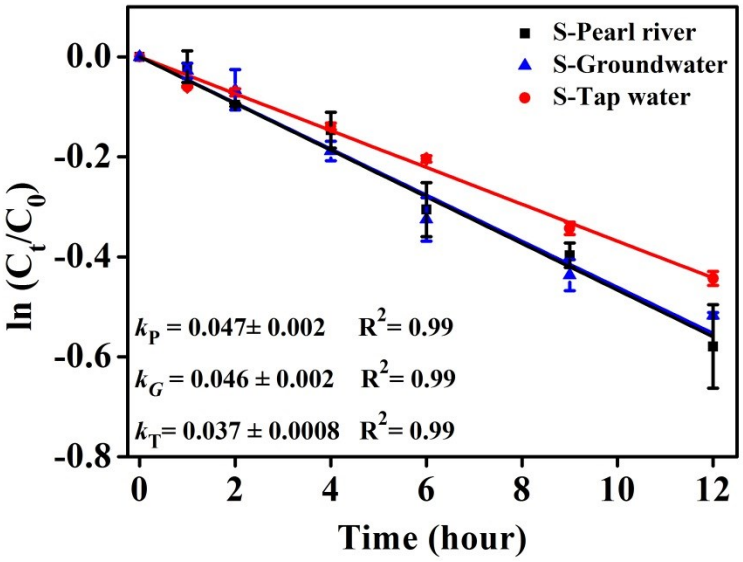

Table S1. Binding energy and relative peak area of XPS peaks of Fe($2p_{3/2}$) and S($2p_{3/2}$) elements on the surface of nZVI and S-nZVI^{S} samples

Sample	Species		B.E（eV）	Relative peak area（%）
nZVI	Fe($2p_{3/2}$)	Fe^0	706.5	16.94
		Fe(II)-O	710.1	63.32
		Fe(III)-O	713.5	19.74
S-nZVI-0.015	Fe($2p_{3/2}$)	Fe^0/ Fe(II)-S	706.7	15.68
		Fe(II)-S	707.4	34.29
		Fe(II)-O	709.8	43.22
		Fe(III)-O	712.9	6.81
	S($2p_{3/2}$)	S^{2-}	161.4	62.42
		S_2^{2-}	162.5	37.58
S-nZVI-0.025	Fe($2p_{3/2}$)	Fe^0/ Fe(II)-S	706.8	16.57
		Fe(II)-S	707.6	37.63
		Fe(II)-O	709.8	36.30
		Fe(III)-O	712.6	9.50
	S($2p_{3/2}$)	S^{2-}	161.4	62.65
		S_2^{2-}	162.6	37.35
S-nZVI-0.05	Fe($2p_{3/2}$)	Fe^0/ Fe(II)-S	706.9	8.09
		Fe(II)-S	707.6	30.45
		Fe(II)-O	709.4	49.54
		Fe(III)-O	712.5	11.92

Sample	Species		B.E （eV）	Relative peak area（%）
S-nZVI-0.05	$S(2p_{3/2})$	S^{2-}	161.6	61.60
		S_2^{2-}	162.8	38.40
S-nZVI-0.1	$Fe(2p_{3/2})$	Fe^0/ Fe(II)-S	706.8	7.97
		Fe(II)-S	707.6	18.07
		Fe(II)-O	708.8	59.99
		Fe(III)-O	712.0	13.97
	$S(2p_{3/2})$	S^{2-}	161.4	60.09
		S_2^{2-}	162.4	39.91
S-nZVI-0.25	$Fe(2p_{3/2})$	Fe^0/ Fe(II)-S	706.6	6.82
		Fe(II)-S	707.3	30.59
		Fe(II)-O	709.0	49.24
		Fe(III)-O	712.2	13.35
	$S(2p_{3/2})$	S^{2-}	161.7	69.56
		S_2^{2-}	163.1	30.44

Table S2. Theoretical and actual S/Fe and relative atomic percentage of Fe, S, O, and C of S-nZVI^{S} at different S/Fe molar ratios.

Theoretical S/Fe	Actual S/Fe	Atomic ratio (%)			
		Fe	S	O	C
0	0	62.69	N	4.89	32.42
0.015	0.012	83.39	1.01	3.21	12.39
0.025	0.023	68.41	1.62	3.30	26.68
0.05	0.038	60.17	2.31	5.80	31.71
0.1	0.07	72.18	5.06	5.42	17.33
0.25	0.13	62.91	8.25	6.47	22.37

N: Not detectable

Table S3. Summary of parameters obtained from fitting HER data with the First-order passivation of Fe^0 model with k as global.

S/Fe	A (mmol)	k (h^{-1})	Reduced χ^2	R^2
0	0.96 ± 0.15	0.05 ± 0.01	0.002	0.94
0.025	0.79 ± 0.12			
0.25	0.41 ± 0.08			

Table S4. Summary of parameters obtained from fitting HER data with the Replacement of reactive phases model with $k_{H_2,1}/k_{H_2,2}$ and k as global.

S/Fe	$k_{H_2,1}/k_{H_2,2}$	$S_{1,0} \cdot k_{H_2,2}$ (mmol $\cdot h^{-1}$)	k (h^{-1})	Reduced χ^2	R^2
0	10.86 ± 4.57	0.02 ± 8.54E-4	2.04 ± 1.06	3.34E-4	0.99
0.025		0.02 ± 7.5E-4			
0.25		0.01 ± 5.53E-4			

Table S5. Summary of parameters obtained from fitting HER data with the Advanced phase replacement model with k_1 and k_2 as global.

S/Fe	$k_{H_2,1} / k_{H_2,2}$	$S_{1,0} \cdot k_{H_2,2}$ (mmol $\cdot h^{-1}$)	k_1 (h^{-1})	k_2 (h^{-1})	Reduced χ^2	R^2
0	9.61 ± 4.31	0.02 ± 0.005	1.80± 1.18	1E-4 ± 0.01	4.42E-4	0.99
0.025		0.02 ± 0.004				
0.25		0.01 ± 0.002				

Table S6. Summary of parameters obtained from fitting HER data with the Independent changes in two reactive phases with k_1 and k_2 as global.

S/Fe	A (mmol)	k_1 (h^{-1})	B (mmol)	k_2 (h^{-1})	Reduced χ^2	R^2
0	0.096 ± 0.017	3.38 ± 5.24	19.77 ± 131.95	0.001 ± 0.01	3.05E-4	0.99
0.025	0.096 ± 0.015		15.05 ± 100.41			
0.25	0.044 ± 0.012		8.20 ± 54.73			

Table S7. Performance parameters of Tafel Curves for nZVI and S-nZVI^{S}.

S/Fe ratio	0	0.025	0.25
E_{corr} (mV)	-754	-899	-882
I_{corr} ($\mu A \cdot cm^{-2}$)	0.98	12.47	1.76
b_c (V/dec)	0.23	0.11	0.12
b_a (V/dec)	0.17	0.10	0.09
R_p ($10^4 \Omega \cdot cm^2$)	4.62	0.18	1.27

Table S8. Parameters of cyclic voltammetry curves for nZVI and S-nZVI^{S}.

S/Fe ratios	0	0.025	0.25
Anode potential (mV)	-62	-48	-42
Cathode potential (mV)	-368	-411	-385
Potential difference △V (mV)	-306	-363	-343
Mid-point potential (mV)	-215	-229.5	-213.5
Anode current ($\mu A \cdot cm^{-2}$)	2.04	7.56	2.32
Cathode current ($\mu A \cdot cm^{-2}$)	-3.13	-13.45	-6.45

Table S9. Pseudo first-order rate constants (k_{obs}) for TBBPA removal by S-nZVI^{S}.

Samples	k_{obs} (h^{-1})	R^2
nZVI	0.13 ± 0.008	0.98
S-nZVI$^{S\text{-}0.015}$	0.27 ± 0.015	0.99
S-nZVI$^{S\text{-}0.025}$	1.19 ± 0.071	0.98
S-nZVI$^{S\text{-}0.05}$	0.74 ± 0.066	0.96
S-nZVI$^{S\text{-}0.1}$	0.13 ± 0.023	0.86
S-nZVI$^{S\text{-}0.25}$	0.01 ± 0.0002	0.99
S-nZVI$^{Na_2S_2O_4\text{-}0.015}$	0.04 ± 0.003	0.97
S-nZVI$^{Na_2S_2O_4\text{-}0.025}$	0.03 ± 0.001	0.99
S-nZVI$^{Na_2S_2O_4\text{-}0.05}$	0.01 ± 0.002	0.85
S-nZVI$^{Na_2S_2O_4\text{-}0.1}$	0.02 ± 0.0009	0.99
S-nZVI$^{Na_2S_2O_4\text{-}0.5}$	0.38 ± 0.02	0.99
S-nZVI$^{Na_2S_2O_4\text{-}0.75}$	0.30 ± 0.03	0.98
S-nZVI$^{Na_2S\text{-}0.015}$	0.11 ± 0.006	0.99
S-nZVI$^{Na_2S\text{-}0.025}$	0.16 ± 0.018	0.94
S-nZVI$^{Na_2S\text{-}0.05}$	0.11 ± 0.005	0.99
S-nZVI$^{Na_2S\text{-}0.1}$	0.03 ± 0.003	0.97
S-nZVI$^{Na_2S\text{-}0.3}$	0.05 ± 0.002	0.99
S-nZVI$^{Na_2S\text{-}0.5}$	0.01 ± 0.007	0.14
S - nZVI$^{S\,-\,0.025}_{P}$	0.047± 0.002	0.99
S - nZVI$^{S\,-\,0.025}_{G}$	0.046 ± 0.002	0.99
S - nZVI$^{S\,-\,0.025}_{T}$	0.037 ± 0.0008	0.99

Table S10. Physicochemical properties of water samples.

Physicochemical property	Unit	Ultrapure water	Tap water	Groundwater	Pearl River
pH	-	6.86	6.57	5.75	6.83
Conductivity	$\mu S\ cm^{-1}$	0.76	123.4	161.9	171.0
Na^+	$mg\ L^{-1}$	0	0.16	0.18	0.13
K^+	$mg\ L^{-1}$	0	0.004	0.01	0.02
Mg^{2+}	$mg\ L^{-1}$	0	0.08	0.09	0.09
Ca^{2+}	$mg\ L^{-1}$	0	0.20	0.24	0.39
F^-	$mg\ L^{-1}$	0.16	1.09	1.82	1.61
Cl^-	$mg\ L^{-1}$	0.1	19.29	41.84	14.52
NO_2^-	$mg\ L^{-1}$	0	0.2	0.21	0.45
Br^-	$mg\ L^{-1}$	0	0	0.04	0
NO_3^-	$mg\ L^{-1}$	0.09	3.94	9.43	5.52
SO_4^-	$mg\ L^{-1}$	0.25	8.36	7.20	19.19
NH_4^+-N	$mg\ L^{-1}$	0	0	0	1.83
TN	$mg\ L^{-1}$	0	4.21	9.64	7.8
TP	$mg\ L^{-1}$	0	0	0	0.23
BOD_5	$mg\ L^{-1}$	0	0	0	3
COD	$mg\ L^{-1}$	0	3.95	6.32	18.57

References

1. S. R. Rajajayavel and S. Ghoshal, Enhanced reductive dechlorination of trichloroethylene by sulfidated nanoscale zerovalent iron, *Water Res.*, 2015, **78**, 144-53, DOI: 10.1016/j.watres.2015.04.009.
2. Y. M. Su, A. S. Adeleye, A. A. Keller, Y. X. Huang, C. M. Dai, X. F. Zhou and Y. L. Zhang, Magnetic sulfide-modified nanoscale zerovalent iron (S-nZVI) for dissolved metal ion removal, *Water Res.*, 2015, **74,** 47-57, DOI: http://dx.doi.org/10.1016/j.watres.2015.02.004.
3. D. Fan, R. P. Anitori, B. M. Tebo, P. G. Tratnyek, J. S. Lezama Pacheco, R. K. Kukkadapu, M. H. Engelhard, M. E. Bowden, L. Kovarik and B. W. Arey, Reductive sequestration of pertechnetate ($^{99}TcO_4^-$) by nano zerovalent iron (nZVI) transformed by abiotic sulfide, *Environ. Sci. Technol.*, 2013, **47**, 5302-10, DOI: 10.1021/es304829z.
4. H. Qin, X. H. Guan, J. Z. Bandstra, R. L. Johnson and P. G. Tratnyek, Modeling the kinetics of hydrogen formation by zerovalent iron: Effects of sulfidation on micro- and nano-scale particles, *Environ. Sci. Technol.*, 2018, **52**, 13887-13896, DOI: 10.1021/acs.est.8b04436.